Theory of supervirtual refraction interferometry

Pawan Bharadwaj,[1,2] Gerard Schuster,[1] Ian Mallinson[1] and Wei Dai[1]

[1]*King Abdullah University of Science and Technology, Thuwal, Saudi Arabia*
[2]*Indian School of Mines, Dhanbad, India. E-mail: gerard.schuster@kaust.edu.sa*

SUMMARY

Inverting for the subsurface velocity distribution by refraction traveltime tomography is a well-accepted imaging method by both the exploration and earthquake seismology communities. A significant drawback, however, is that the recorded traces become noisier with increasing offset from the source position, and so accurate picking of traveltimes in far-offset traces is often prevented. To enhance the signal-to-noise ratio (SNR) of the far-offset traces, we present the theory of supervirtual refraction interferometry where the SNR of far-offset head-wave arrivals can be theoretically increased by a factor proportional to $\sqrt{N}$; here, N is the number of receiver or source positions associated with the recording and generation of the head-wave arrival. There are two steps to this methodology: correlation and summation of the data to generate traces with virtual head-wave arrivals, followed by the convolution of the data with the virtual traces to create traces with supervirtual head-wave arrivals. This method is valid for any medium that generates head-wave arrivals recorded by the geophones. Results with both synthetic traces and field data demonstrate the feasibility of this method.

There are at least four significant benefits of supervirtual interferometry: (1) an enhanced SNR of far-offset traces so the first-arrival traveltimes of the noisy far-offset traces can be more reliably picked to extend the useful aperture of the data, (2) the SNR of head waves in a trace that arrive later than the first arrival can be enhanced for accurate traveltime picking and subsequent inversion by later-arrival traveltime tomography, (3) common receiver-pair gathers can be analysed to detect the presence of diving waves in the first arrivals, which can be used to assess the nature of the refracting boundary, and (4) the source statics term is eliminated in the correlation operations so that the timing of the virtual traces is independent of the source excitation time. This suggests the possibility of applying this method to earthquake data recorded by receivers that are inline with the refraction paths and source locations.

Key words: Interferometry; Interface waves.

1 INTRODUCTION

Geophysicists have used wide-angle refraction surveys to image the gross crustal velocity structure of the Earth (Mooney & Weaver 1989; Zelt & Smith 1992; Sheriff & Geldart 1995; Funck *et al.* 2008), as well as the detailed structure within the first few hundred metres of the near surface (Zhu *et al.* 1992). For wide-angle marine crustal studies, only a small number of Ocean Bottom Seismometers (OBS), often fewer than 100, are deployed while the source boat shoots at hundreds of shot points over a long range of offsets; the source–receiver offsets for OBS surveys can range from kilometres to tens of kilometres. Even fewer recording stations are sometimes deployed for a sonobuoy array.

An improvement of the refraction method was proposed by Palmer (1981) as the generalized reciprocal method (GRM). The refraction traveltimes are resorted to give traveltimes for a pair of geophones, which are then used for refractor velocity analysis and time-depth calculations. Later, Palmer & Jones (2005) combined the GRM with convolution operations as means for estimating refraction statics in which there are large and rapid variations in the depth of weathering.

A significant problem with current refraction surveys is that they usually require very strong sources in order to record first arrivals with high signal-to-noise ratio (SNR) at the far-offset traces. Without a sufficiently high SNR in the far-offset traces, the refraction traveltimes cannot accurately be picked. To partly overcome this problem, Dong *et al.* (2006) developed the theory of refraction interferometry to increase the SNR of head-wave arrivals. As illustrated in Fig. 1(a), this method windows about the head-wave arrivals and correlates a pair of traces to give $\phi_x(\mathbf{A}, \mathbf{B}, t)$, where $\mathbf{A}$ and $\mathbf{B}$ are the geophone positions and $\mathbf{x}$ is the source position; the resulting virtual trace contains a virtual refraction arrival with the arrival time of $\tau_{\mathrm{A'B}} - \tau_{\mathrm{A'A}}$. Repeating this procedure for any post-critical source position and the same geophone pair at $\mathbf{A}$ and

a). Crosscorrelate and stack over x to generate virtual refractions

b). Convolve and stack over A to generate super−virtual refractions

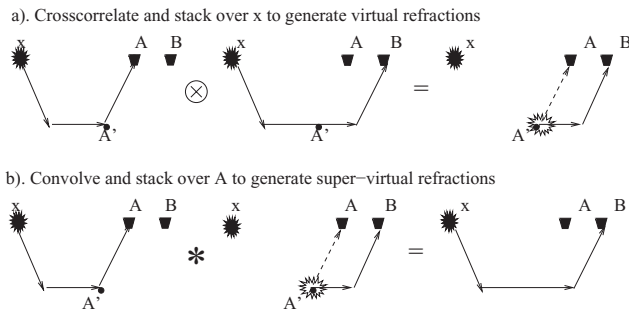**Figure 1.** The steps for creating supervirtual refraction arrivals. (a) Correlation of the recorded trace at **A** with that at **B** for a source at **x** to give the trace $\phi_x(\mathbf{A}, \mathbf{B}, t)$ with the virtual refraction with the traveltime denoted by $\tau_{A'B} - \tau_{A'A}$. This arrival time will be the same for all post-critical source positions, so stacking $\sum_x \phi_x(\mathbf{A}, \mathbf{B}, t)$ will enhance the SNR of the virtual refraction by $\sqrt{N}$. (b) Similar to that in (a) except the virtual refraction traces are convolved with the actual refraction traces and stacked for different geophone positions at A to give the supervirtual trace at B with a SNR enhanced by an additional $\sqrt{N}$; however, this potential enhancement is spoiled by the fact that, prior to stacking, the noisy raw trace is convolved with the relatively clean virtual trace to produce a noisy trace again. Solid (dashed) rays are associated with positive (negative) traveltimes. Similar to migration and demigration in seismic imaging, (a) represents kinematically datuming the surface source at **x** to the subsurface location at **A'**, and (b) represents *detauming* the source at **A'** to the surface location at **x**.

B will lead to a virtual trace with the same refraction traveltime; hence, stacking the correlated trace $\phi_x(\mathbf{A}, \mathbf{B}, t)$ over all post-critical source positions **x** will yield traces with virtual-refraction events of higher SNR. This enhancement can be as high as $\sqrt{N}$, where N is the number of sources that generates this particular head wave. They demonstrated this method on seismic data shot over a salt dome in Utah, and later Nichols *et al.* (2010) demonstrated its effectiveness over a hydro geophysical research site in Idaho.

A problem with this approach to refraction interferometry is that the virtual head-wave trace has an unknown excitation time[1], even though it has the correct moveout pattern. Another problem is that correlation of traces typically decreases the source–receiver offset of the virtual trace because traveltimes are subtracted and are associated with shorter ray paths (Schuster 2009). To overcome these problems, Bharadwaj & Schuster (2010), Mallinson (2010) and Mallinson *et al.* (2011) presented an extension of refraction interferometry so that the receiver spread could be extended to its maximum recording extent and the absolute arrival time is properly accounted for. This new method creates virtual far-offset refraction arrivals by a combination of both correlation (Fig. 1a) and convolution (Fig. 1b) of traces with one another to create what is denoted as supervirtual refraction traces. Mallinson *et al.* (2011) presented the work flow for supervirtual refraction interferometry (SVI) and demonstrated its effectiveness with both synthetic and field data results, but only gave an intuitive explanation of its underlying principles. In our new paper, we present the rigorous theory of SVI.

The two steps of correlation–convolution were proposed by Curtis (2009) and Curtis & Halliday (2010) as a means to partly recover the boundary data when the scattering medium and/or source–receiver geometry are insufficient. Instead of just one

---

[1] It was suggested in Dong *et al.* (2006) that the unknown excitation time can be reset to zero time by setting the traveltime of the virtual stacked refraction trace to the traveltime of the corresponding recorded trace with high SNR.

boundary contour the two-step procedure is implemented with two boundaries, one containing the other. A motivation for this procedure is that the correlation operation in the frequency domain subtracts phases from the two traces to yield a virtual trace with a phase term smaller in magnitude than one of the input traces, as shown on the right-hand side of Fig. 1(a). Smaller values of the phase magnitude are related to shorter ray paths, so recovering the longest ray path events from correlated traces truncated in time and the recording aperture will be impossible. However, if these short-ray path virtual traces are convolved with the actual traces then their phases are added together in the frequency domain to create events with longer ray paths, as shown on the right side of Fig. 1(b). Poliannikov (2011) demonstrated the feasibility of this approach with synthetic data where the reflections from a structure were constructed using several events produced simultaneously by two stationary sources. An earlier example of using the combined correlation-convolution operation is the iterative least-squares solution for redatuming seismic data (Xue & Schuster 2008), which is a concatenation of correlation (datuming) and convolution (modelling or dedatuming) operations, but in this case the residual traces rather than the recorded traces are used as the input.

The first part of this paper presents the rigorous theory of SVI. This is followed by examples using synthetic data and OBS field records that demonstrate the effectiveness of SVI and its $\sqrt{N}$ enhancement of the SNR. The last section presents a summary.

2 THEORY

We will first present the far-field reciprocity equations of correlation and convolution types, and then show how they can be used to construct supervirtual refractions. The use of the far-field reciprocity equation to create virtual refractions and enhance their SNR was presented by Dong *et al.* (2006), but convolving virtual traces with refraction data to create long-offset refraction traces is the key innovation in our paper. The theory for this convolution step is consistent with that described in Curtis & Halliday (2010). We will assume an acoustic medium with an arbitrary velocity distribution with constant density, and wide-band sources with unity amplitude at each frequency.

2.1 Reciprocity equations of correlation type

Assume a source at **x** in Figs 1(a) and 2(a) and receivers at **A** and **B**. The reciprocity theorem of correlation type (Wapenaar & Fokkema 2006) states that the virtual Green's function $G(\mathbf{A}|\mathbf{B})^{\text{virt.}}$ is given by

$$\mathbf{B}, \mathbf{A} \in V_0; 2i\,Im[G(\mathbf{A}|\mathbf{B})^{\text{virt.}}]$$
$$= \int_{\text{top}} [G(\mathbf{B}|\mathbf{x})^* \frac{\partial_x G(\mathbf{A}|\mathbf{x})}{\partial n} - G(\mathbf{A}|\mathbf{x}) \frac{\partial_x G^*(\mathbf{B}|\mathbf{x})}{\partial n}] d^2 x, \quad (1)$$

where $\frac{\partial_x G(\mathbf{B}|\mathbf{x})}{\partial n} = \nabla G(\mathbf{B}|\mathbf{x}) \bullet \hat{n}$ for the outward unit normal $\hat{n}$ on the boundary. Here, the Green's function solves the Helmholtz equation for an arbitrary velocity distribution with a constant density (we follow the notation from Schuster (2009)). The integration path is only over the top path as the half-circle path is neglected by the Wapenaar antiradiation condition.

To avoid artefacts due to a limited recording aperture and discrete sampling, Dong *et al.* (2006) suggested windowing about the first arrivals so that only head wave arrivals are correlated with one another. In this case, $G(\mathbf{A}|\mathbf{B})$ is replaced by the head-wave arrival
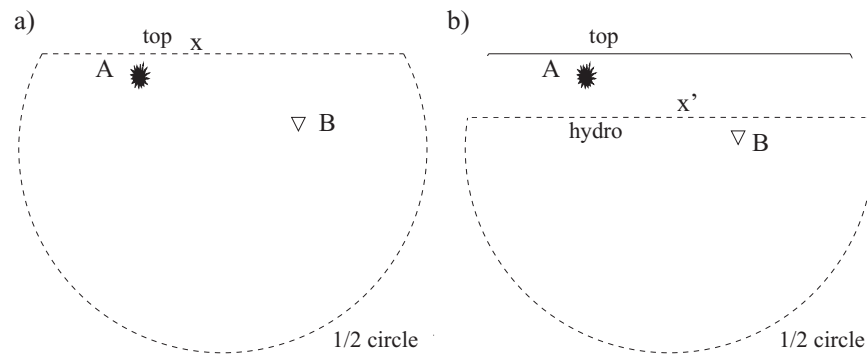
a)

top   x

A ✹

▽ B

1/2 circle

b)

top

A ✹

x'

hydro   ▽ B

1/2 circle

Figure 2. (a) Geometry for computing virtual Green's functions $G(\mathbf{A}|\mathbf{B})$ from the recorded data $G(\mathbf{A}|\mathbf{x})$ and $G(\mathbf{B}|\mathbf{x})$ using the reciprocity theorem of correlation type in an arbitrary acoustic medium of constant density. (b) Geometry for computing supervirtual Green's functions $G(\mathbf{B}|\mathbf{A})^{\text{super}}$ from the recorded data $G(\mathbf{A}|\mathbf{x}')$ and the virtual data $G(\mathbf{B}|\mathbf{x}')^{\text{virt.}}$ using the reciprocity theorem of convolution type. The above diagrams are valid for 3-D by extending the semi-circular surface to that of a hemisphere.
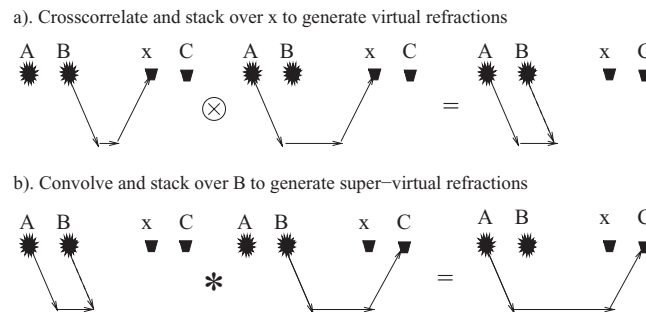
a). Crosscorrelate and stack over x to generate virtual refractions

A B   x C   A B   x C   A B   x C

⊗   =

b). Convolve and stack over B to generate super−virtual refractions

A B   x C   A B   x C   A B   x C

∗   =

Figure 3. Same as Fig. 1 except long-offset refractions are created from shorter-offset refractions.

term defined as $\mathcal{G}(\mathbf{A}|\mathbf{B})$ to give under the far-field approximation[2]

$$Im[\mathcal{G}(\mathbf{A}|\mathbf{B})^{\text{virt.}}] \approx k \int_{\text{top}} \mathcal{G}(\mathbf{A}|\mathbf{x})^* \mathcal{G}(\mathbf{B}|\mathbf{x}) d^2 x, \qquad (2)$$

where k is the average wavenumber and $\mathcal{G}(\mathbf{A}|\mathbf{B}) = G(\mathbf{A}|\mathbf{B})^{\text{head}}$ represents the head wave contribution in the Green's function for a specific interface.[3] This approximation is somewhat analogous to that used in redatuming reflection data to a new datum where $\mathcal{G}(\mathbf{A}|\mathbf{x})$ is a model-based extrapolation Green's function that only accounts for direct arrivals, and $\mathcal{G}(\mathbf{x}|\mathbf{B})$ represents the refraction data devoid of direct waves and multiples.

According to the ray diagram in Fig. 1(a), the correlated trace[4] $\mathcal{F}^{-1}[\mathcal{G}(\mathbf{A}|\mathbf{x})^* \mathcal{G}(\mathbf{B}|\mathbf{x})]$ for a source at $\mathbf{x}$ has the same kinematics as the correlated trace $\mathcal{F}^{-1}[\mathcal{G}(\mathbf{A}|\mathbf{x}')^* \mathcal{G}(\mathbf{B}|\mathbf{x}')]$ for a source[5] at $\mathbf{x}'$; here $\mathbf{x}'$ (not shown) is another source position post-critically offset from the receiver pair. Such sources are considered to be at stationary points (Snieder 2004), and similar to surface wave inter-

ferometry (Halliday & Curtis 2008; Xue *et al.* 2009) or diffraction wave interferometry (Dai *et al.* 2011), stacking of the virtual traces tends to enhance the SNR of the virtual head-wave arrival (Yilmaz 2001; Dong *et al.* 2006) by a factor of $\sqrt{N}$. Here, N represents the number of source positions that generate this type of head wave and additive white noise is assumed.

2.2 Reciprocity equations of convolution type

It is assumed that the virtual data $G(\mathbf{B}|\mathbf{A})^{\text{virt.}}$ can be extrapolated to get $G(\mathbf{x}'|\mathbf{A})^{\text{virt.}}$ for $\mathbf{x}'$ along the horizontal dashed line in Fig. 2(b); similarly, the field data can be extrapolated to get $G(\mathbf{x}'|\mathbf{B})$. In this case, the reciprocity theorem of convolution type (Slob *et al.* 2007; Wapenaar 2007) can then be employed
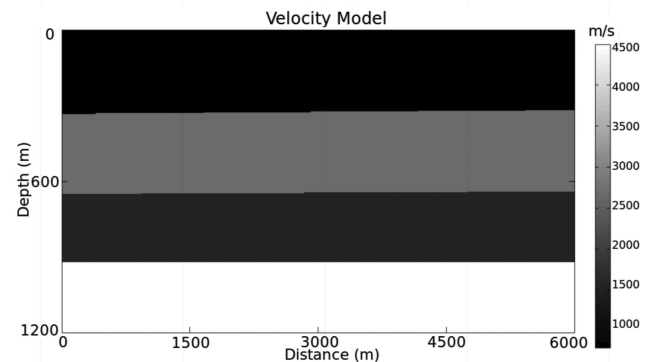
Velocity Model

m/s

Depth (m)

Distance (m)

Figure 4. Acoustic velocity model used for generating the synthetic CSG in Fig. 5(b). The source and recording lines are 15 m beneath the free surface and the source wavelet is a Ricker wavelet with a peak frequency of 15 Hz. The 59 sources and 250 receivers are spaced at 15 m intervals.

---

[2] For a marine survey, the $G(\mathbf{A}|\mathbf{x})$ can be recorded by towed hydrophones (or ocean bottom seismometers) positioned beneath the sources at $\mathbf{x}\epsilon$ top. To satisfy the far-field approximation, it is assumed that the down going ghosts from the free surface have largely been removed. We have implicitly assumed that the source wavelet amplitude is zero phase and has the amplitude value of 1. More generally, the wavelet power spectrum can be included to take into account source wavelet effects.

[3] Causality demands that the real part of the Green's function is related to the Hilbert transform of the imaginary part (Wapenaar 2004). Once the imaginary part of the Green's function is obtained, the real part can be computed by a Hilbert transform.

[4] $\mathcal{F}^{-1}$ denotes the temporal inverse Fourier transform.

[5] This assumes that the two sources are beyond the critical offset and the head waves emerge from the same refracting boundary.
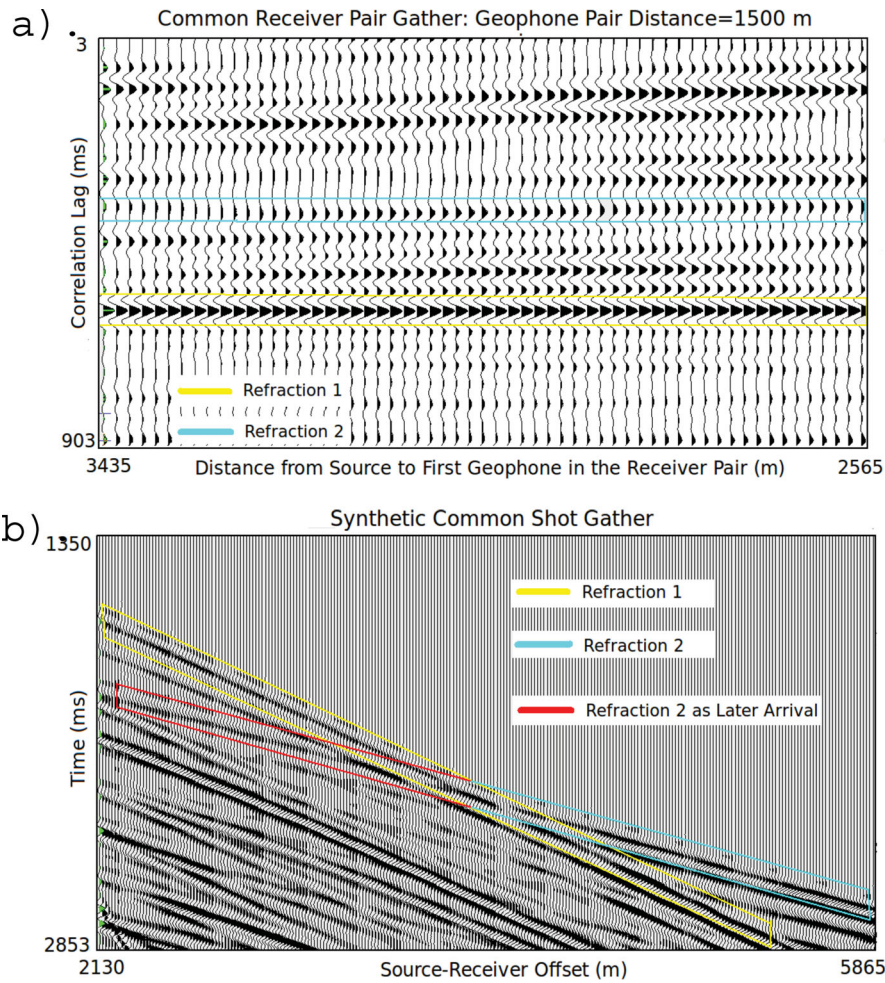
a)

Common Receiver Pair Gather: Geophone Pair Distance=1500 m

— Refraction 1
— Refraction 2

Correlation Lag (ms)

Distance from Source to First Geophone in the Receiver Pair (m)

b)

Synthetic Common Shot Gather

— Refraction 1
— Refraction 2
— Refraction 2 as Later Arrival

Time (ms)

Source-Receiver Offset (m)

Figure 5. (a) CPG where the receivers are separated by 1500 m. Horizontal events in this gather will represent head-wave refractions even if the refracting boundary is irregular. (b) A synthetic CSG with a surface source located 165 m from the upper left corner of the Fig. 1 velocity model. First arrivals (yellow and blue lines) and later refraction arrivals before the cross-over offset (red lines) are highlighted.

$$G(\mathbf{B}|\mathbf{A}) =$$

$$\int_{\text{hydro}} [G(\mathbf{B}|\mathbf{x}') \frac{\partial_{\mathbf{x}'} \mathbf{G}(\mathbf{A}|\mathbf{x}')}{\partial \mathbf{n}} - \mathbf{G}(\mathbf{A}|\mathbf{x}') \frac{\partial_{\mathbf{x}'} \mathbf{G}(\mathbf{B}|\mathbf{x}')}{\partial \mathbf{n}}] \mathbf{d}^2 \mathbf{x}', \quad (3)$$

where the integration is along the hydro dashed line in Fig. 2(b) and the integration along the half-circle is negligible by the Sommerfeld radiation condition. Assuming the far-field approximation and setting $G \to \mathcal{G}$ yields the expression for the trace with the supervirtual head wave

$$\mathcal{G}(\mathbf{B}|\mathbf{A})^{\text{super}} \approx 2ik \int_{\text{hydro}} \mathcal{G}(\mathbf{B}|\mathbf{x}')^{\text{virt.}} \mathcal{G}(\mathbf{A}|\mathbf{x}') d^2 x', \quad (4)$$

where $\mathcal{F}^{-1}[\mathcal{G}(\mathbf{B}|\mathbf{A})^{\text{super}}]$ is the supervirtual trace obtained by convolving the recorded data $\mathcal{F}^{-1}[\mathcal{G}(\mathbf{A}|\mathbf{x}')]$ with the virtual data $\mathcal{F}^{-1}[\mathcal{G}(\mathbf{B}|\mathbf{x}')^{\text{virt.}}]$. Compared to the raw trace, the supervirtual head-wave arrival has a SNR enhanced by the factor $\sqrt{N}$, which means the combined enhancement using both eqs 2 and 4 can be as high as N if the virtual data are convolved with the supervirtual data. However, practical considerations such as artefacts associated with limited recording apertures, discrete source and receiver sampling, windowing of the head waves, geometrical spreading and the far-field approximation will likely prevent the attainment of this ideal enhancement.

In the synthetic section, we will use the example of head waves that have been windowed from the original data so that $G(\mathbf{x}|\mathbf{y}) \approx G(\mathbf{x}|\mathbf{y})^{\text{head}}$, but it will be understood that this procedure is valid for diving waves as well if the time window is opened up to include all arrivals. A desirable property of head waves, similar to that of surface waves (Halliday & Curtis 2008; Xue *et al.* 2009), is that almost every surface source position in the post-critical region is a stationary point for a fixed pair of in-line receivers and a 2-D medium[6]; hence, a virtual head wave is reinforced at almost every inline source position for the specified receiver pair. This is not true if the refraction arrival is a pure diving wave, so the SNR of virtual diving waves will not be greatly increased. The exception is if the refracting interface is a thin layer with a transition velocity governed by a, for example, linear velocity gradient. In this case, interference effects of waves refracting within this zone can greatly increase the amplitudes of the head waves recorded on the surface (Braile & Smith 1975).

[6] For a 3-D recording geometry, the stationary source points associated with a planar refractor and a pair of receivers will only be along a line of sources inline with the receiver pair.
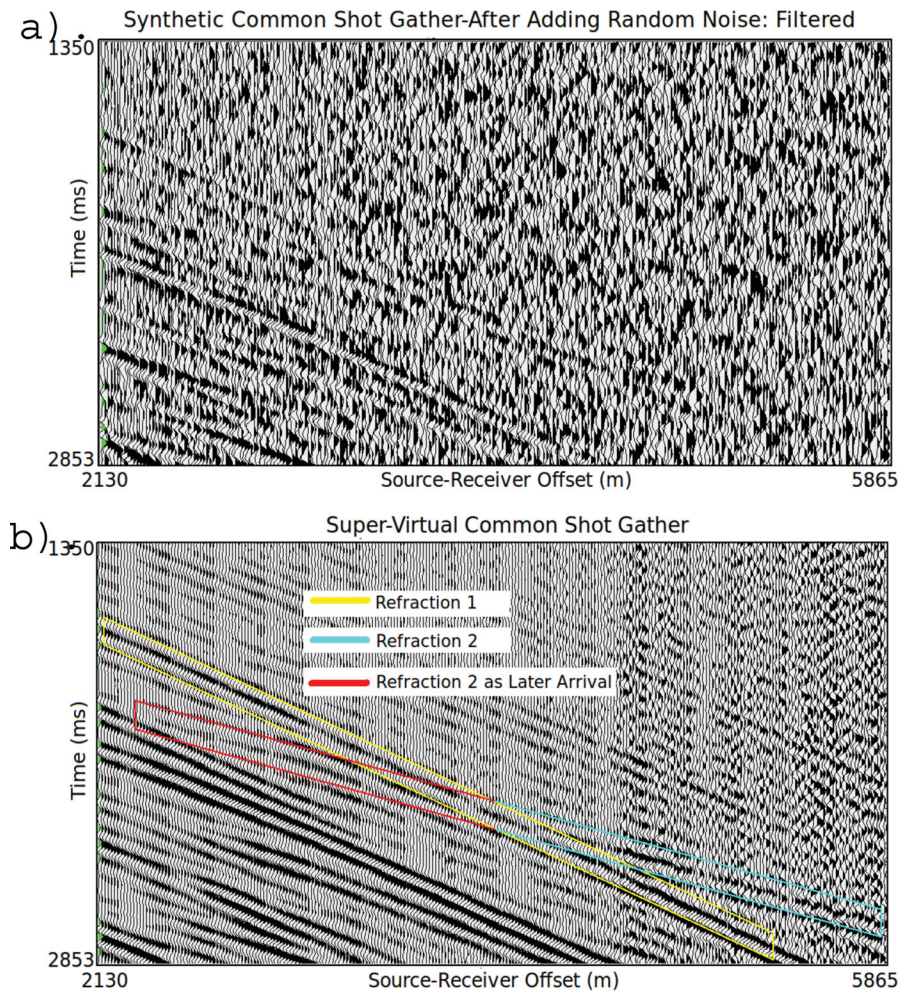
Figure 6. (a) Fig. 5(b) synthetic shot gather after addition of white noise. (b) Supervirtual CSG with an improved SNR. Traveltime picking of first arrivals (blue and yellow lines) and later refraction arrivals (red lines) are greatly enhanced.

2.3 Long-offset refractions from short-offset refractions

Fig. 1 depicts the rays for creating supervirtual long-offset refractions by the convolution and correlation of shorter-offset and long-offset refractions. A possible problem with this approach is that the long-offset refractions might have very low SNR values and so degrade the quality of the final supervirtual refraction. A partial remedy is to only use short-offset refractions with high SNR to create a long-offset trace with a high SNR refraction, as illustrated in Fig. 3. As shown, only short-offset refraction traces are used to create the long-offset supervirtual refraction (see ray diagram on lower right-hand part of Fig. 3b). This is desirable because the shorter-offset arrivals typically have higher SNR values than the longer-offset arrivals.

3 SYNTHETIC DATA EXAMPLE

To demonstrate the effectiveness of SVI, we apply it to synthetic common shot gathers generated by a finite-difference solution to the 2-D acoustic wave equation for the velocity model shown in Fig. 4. A typical common receiver pair gather (CPG) and a shot gather are shown in Fig. 5, with the geophone pair distance[7] equal to 1500 m.

[7] See see Dong *et al.* (2006) for field data examples of a CPG.

White noise is now added to all the synthetic CSGs and a noisy CSG is shown in Fig. 6(a). Here, the SNR of the far-offset traces is as low as 0.2 so that the first arrivals cannot be picked even after bandpass filtering. To rectify this problem, the traces are correlated and summed (see equation 2) to create virtual traces; and then convolving these virtual traces (after dip filtering to eliminate coherent noise) with the raw traces yields, after stacking (see equation 4), the supervirtual traces shown in Fig. 6(b); these traces were also dip filtered to eliminate coherent artefacts.[8] It is obvious that most of the first arrival traveltimes can be now be picked in the supervirtual traces compared to the raw traces in Fig. 6(a). Even refraction arrivals that arrive after the first arrival can be identified in the red box shown in Fig. 6(b).

Artefacts are partly generated by the finite length of the recording geometry and the subsequent truncation of the integration limits;

[8] There are three different processing procedures that might be used to compute supervirtual events with high quality. Procedure 1 is to correlate and stack the raw records to create virtual traces, then convolve these virtual traces with the raw traces and sum over appropriate receiver positions. Procedure 2 is the same as procedure 1 except the raw traces and virtual traces are windowed (window width about two periods long) about the expected first arrivals. Procedure 3 is the same as 1 or 2 except dip filters are used to eliminate unwanted dipping events in both the raw data and virtual data. The traces at and near the shot location should be muted.
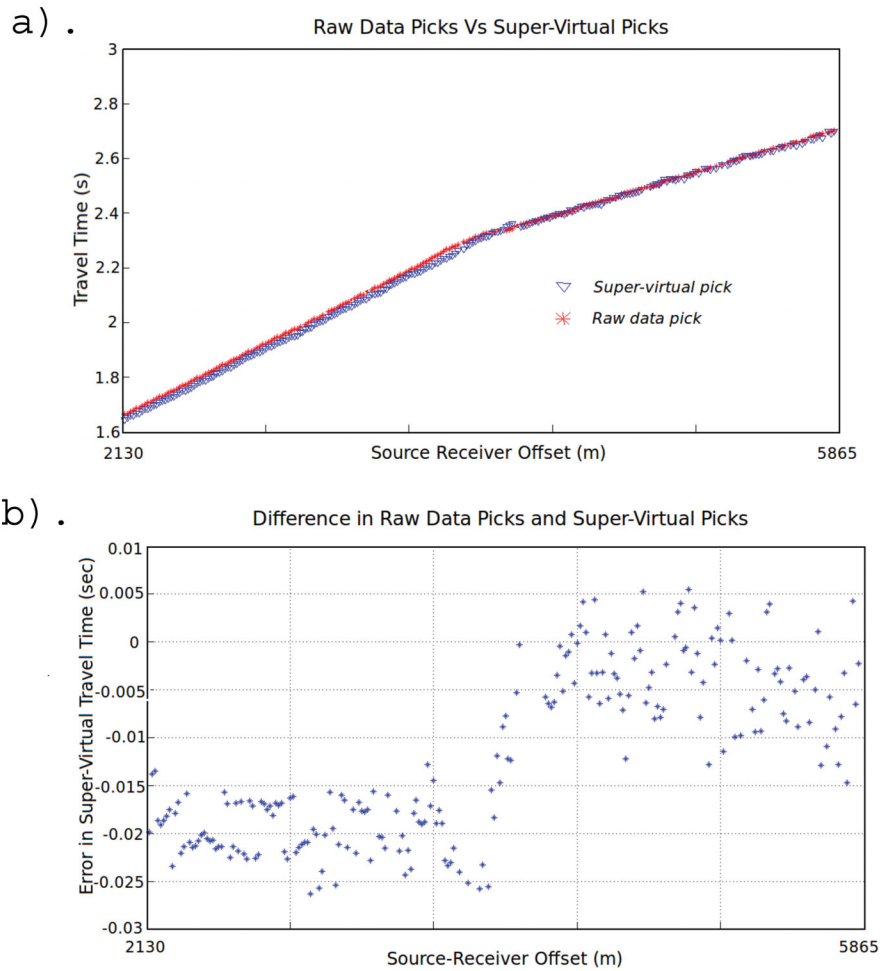
a).

Raw Data Picks Vs Super-Virtual Picks

b).

Difference in Raw Data Picks and Super-Virtual Picks

Figure 7. Plots showing (a) picked traveltimes for the raw traces and supervirtual traces for a synthetic common shot gather and (b) their differences in travel time picks.

also, refractions from different interfaces can correlate with one another and constructively sum together to produce further artefacts. Careful windowing about the arrivals can help reduce these problems, but not eliminate them. Sometimes a better estimate of the window location and length can be obtained after the 1st iteration of the supervirtual method, and so the SVI procedure can be repeated with a refined window design.

To validate the accuracy of the picked traveltimes, first arrival times are picked in the supervirtual gather and Fig. 7(a) compares them to the traveltimes picked from the raw data. The difference in the these traveltimes is mostly within $T/4 = 0.017$ s of each other as shown in Fig. 7(b). This is consistent with the field data results of (Mallinson *et al.* 2011) where more than 90 percent of the picked traveltimes agreed within a quarter of a period of the actual traveltimes for the raw traces with pickable events.

The supervirtual traces are obtained by the correlation and convolution of the raw traces so that the supervirtual source wavelet becomes ringy. This can lead to an ambiguous identification of the first arrival, so that there might be a discrepancy in the picked virtual traveltime with respect to the actual arrival time. This discrepancy can be identified by comparing the supervirtual traveltime to the actual traveltime picked from a trace with a high SNR. Alternatively, the supervirtual traces can be deconvolved by the inverse to the autocorrelation of the wavelet prior to picking. For the field data example to be presented later, a spiking filter ap-

plied to the virtual traces proved to be effective in reducing the ringiness.

3.1 SNR of supervirtual traces

The SNR[9] of first arrivals in the noisy (red) and supervirtual (blue) traces in Fig. 6 are plotted in Fig. 8. Here, white noise is added to the traces and it is expected that stacking N noisy traces will decrease the noise level by a factor proportional to $\sqrt{N}$ (Yilmaz 2001). These supervirtual traces were computed with $N = 17$ shot gathers so the expected improvement in SNR is about $\sqrt{17} = 4.1$. To verify this prediction, an exponential curve $S(T)$ is fitted to the noisy red points in Fig. 8(a) as a function of the trace number T and is plotted as the green curve. We then least-squares fit the equation

$$S(T)' = c1 \cdot S(T) + c2, \qquad (5)$$

to the blue supervirtual points to give $c1$=4.268 and $c2 = 1.387$; the new fitted curve $S'(T) = 4.286S(T)+1.387$ is plotted in yellow. Ideally, the factor $c1$ should be $4.12 \approx \sqrt{N}$ for this supervirtual gather with $N = 17$ and $c2$ should be zero; this means that the actual SNR enhancement of the supervirtual traces is somewhat better than the $\sqrt{N}$ prediction.

---

[9] Signal-to-noise ratio, $SNR = Max.|Signal|/Max.|Noise|$.
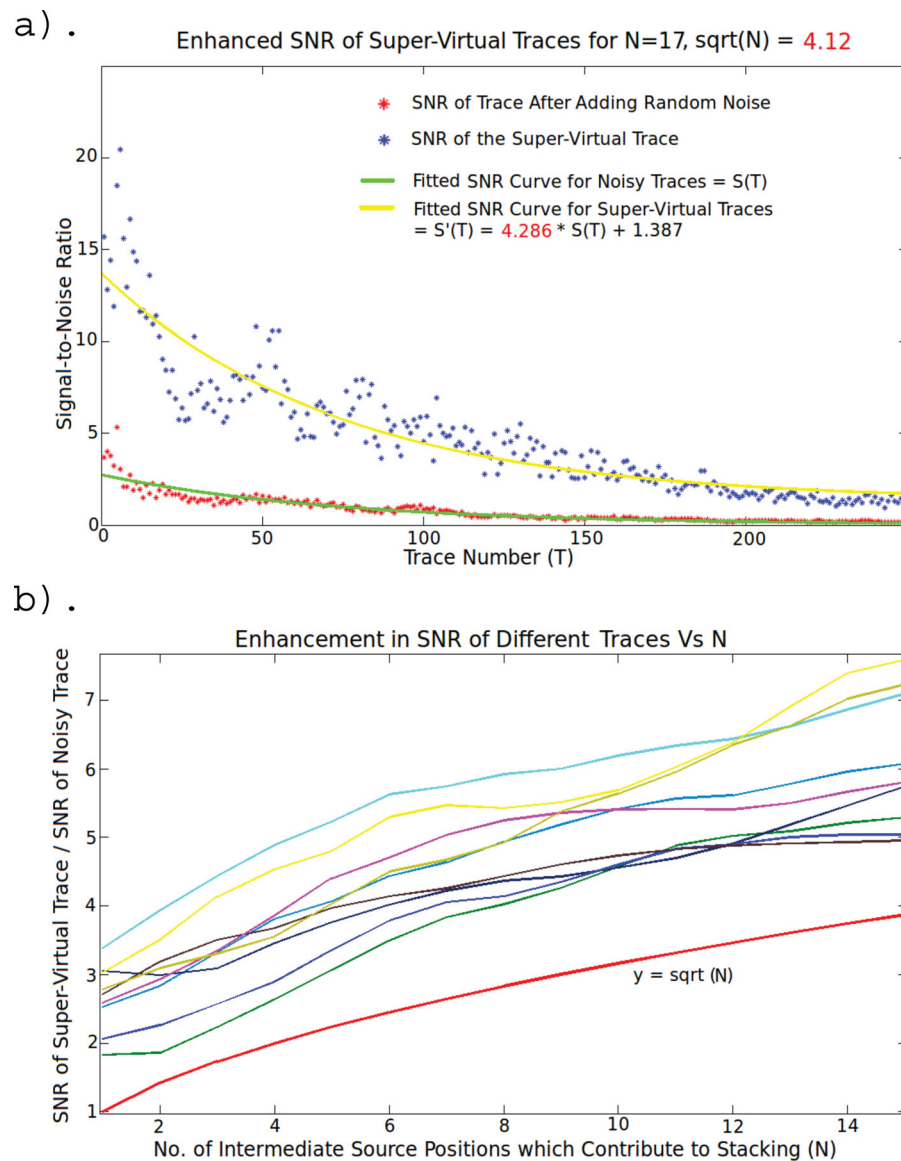
a).

b).

Figure 8. (a) SNR versus T plot of the the noisy (red points) and supervirtual (blue points) traces in Fig. 6; here, T is the trace number. The green curve $S(T)$ is the best fit exponential curve to the red points and the blue curve is that of the best fit function in equation 5. (b) The SNR versus N plot for the supervirtual traces. Here, N is the number of source positions that contribute to the stacked supervirtual trace; for example, $N = 17$ to create the supervirtual traces for the (a) plot.

In Fig. 8(b), the ratio between the SNR of the supervirtual trace and the corresponding noisy trace is plotted against the stack number N. Each coloured curve corresponds to a different trace and generally follows the trend of the red $\sqrt{N}$ versus N curve, except for a constant shift along the vertical axis.

4 OBS DATA RESULTS

We now demonstrate the effectiveness of SVI applied to six ocean bottom seismic (OBS) gathers (see Fig. 9a) collected by a marine survey off the coast of China. Here, the inline OBS station spacing is 15 km and the inline shots are spaced at 150 m intervals. The maximum number of shots for the far-offset OBS is 1516 and the maximum source–receiver offset is 181 km. Fig. 10(a) shows a recorded CRG along with the positions of other stations [marked (ii) to (vi)] in the survey. The recording time of the traces is 30 s, and the traces past 50 km cannot be picked with confidence, even

after the processing steps of bandpass and prediction error filtering. Zoom views of the yellow and red boxes are shown in the top row of Fig. 9 and show no visible first-arrival events that can be picked with confidence. Fortunately, Meissner's (1973) review of Moho data[10] suggests that Moho refractions are likely to exhibit the kinematic properties of head waves, and so enjoy the $\sqrt{N}$ stacking property illustrated in Fig. 8.

To recover these arrivals, the flowchart in Fig. 11 depicts the processing steps for obtaining supervirtual traces, and the details are described below. Many of these steps were used by Mallinson (2010)

[10] Meissner's (1973) review paper concludes that the '...overall picture from different seismic investigations shows the Moho as a laminar transition zone of a few kilometres thickness. There is a general stepwise increase in the velocity of compressional (P) and shear waves (S), possibly often interrupted by layers with lower velocities, until values around 8 km s^{-1} are reached for the P waves in the uppermost part of the mantle.'.
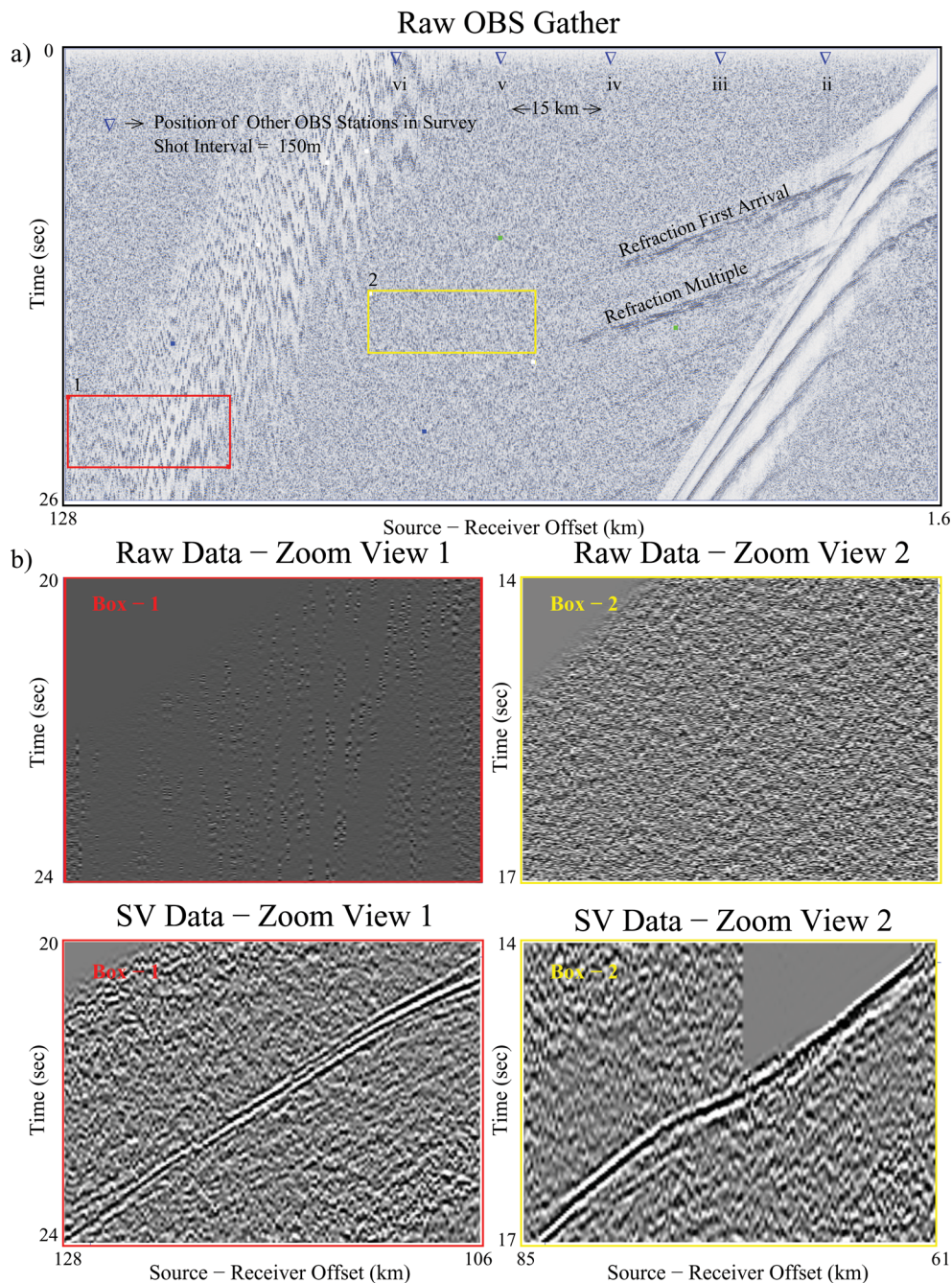
Figure 9. (a) An OBS gather, where both the first arrivals and the refraction multiples are visible only up to a certain source–receiver offset. The positions of other OBS stations are located at 15 km intervals marked by the triangular geophone symbols. (b) Zoomed views at corresponding coloured boxes [1 and 2 in (a)] of both raw and supervirtual data.

to process OBS data from a marine survey over the Seychelles plateaux, but the key steps for success for the China data are in prediction error filtering and careful editing of the CPGs before stacking.

(i) Window around the first arrivals in each OBS gather, where the window width is about 11.4T, where the dominant source period is $T = 0.15$ s.

(ii) Use a 1–3 Hz high-pass filter to help remove low-frequency noise in the data.

(iii) Cross-correlate traces recorded at a pair of receivers and stack over their common source positions **x**, which are the source

positions as in Fig. 1(a); the result is the stacked virtual trace. The position of **x** should be selected such that it is post-critically offset from both stations *A* and *B*. Some traces have spurious coherent noise, so these traces have not been included in the stacking which is a crucial step for success. Around 150 such virtual traces can be stacked in the present data set to give, ideally, a $\sqrt{150} \approx 12$ enhancement of SNR of the virtual refraction.

(iv) Apply spiking decon to the stacked virtual trace to reduce the ringiness in the source wavelet and the ambiguity in picking the virtual refraction arrival time. Window around the peak corresponding to the virtual travel time in these deconvolved traces. This windowed version of the filtered-stacked trace can be
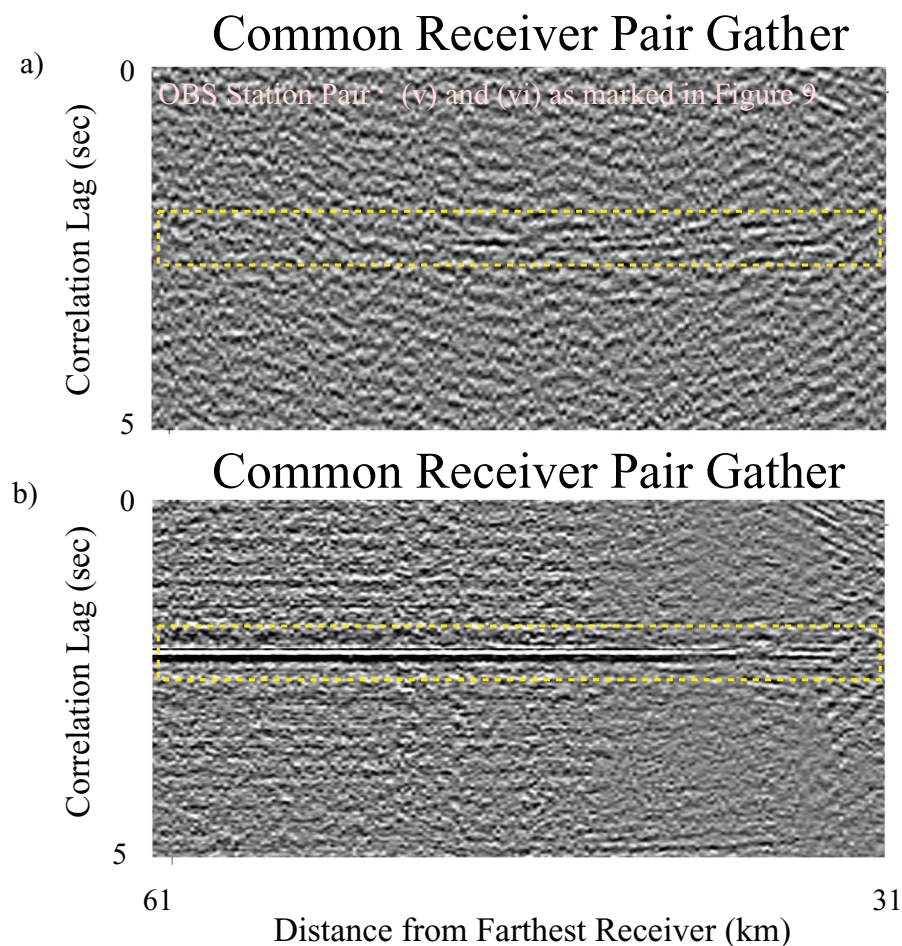
Figure 10. (a) Virtual traces generated after cross-correlation of raw traces at a pair of OBS stations [(v) and (vi), as marked in Fig. 9]. The flat event (yellow box) is not clearly visible because the SNR of raw traces at station (v) is low. (b) Same as (a) except for corresponding SV gather instead of raw gather at station (v) is used for the cross-correlation.

convolved with the corresponding recorded traces to get supervirtual traces.

(v) The stacked virtual trace at **B** is convolved with the field trace $G(\mathbf{A}|\mathbf{x})$, and this result is summed over the receiver positions at **A** in Fig. 1(b). The field trace is PEF filtered and windowed about the expected first arrival with a window length of 3.4 T.

(vi) All of the above steps can be repeated for different receiver positions **A** to generate N_g virtual traces, which can then be stacked together. Here, N_g is the number of geophones post-critically offset from the source.

The above steps are used to generate the supervirtual traces shown in the bottom row of Fig. 9(b). Here, the first arrivals are clearly visible for most traces and can be picked and used for tomographic inversion. In fact, the supervirtual traces in the bottom CRG of Fig. 10 shows that first arrivals can be picked at most of the source–receiver offsets $X > 50$ km compared to the unpickable traces in raw CRG at these offsets. The extra processing steps not used in the synthetics are that CPGs were edited for bad traces and a prediction error filter was applied to the data before the correlation and convolution operations.

As shown in the synthetic example, artefacts can be generated that masquerade as actual first arrivals. To assist in distinguishing artefacts form true first arrivals in Fig. 9(b), a series of tests should be carried out.

(i) Perform simulations on synthetic data for a model that roughly resembles the actual crustal model and acquisition geometry. If the predicted first arrivals match the actual ones then this part of the test has been passed.

(ii) Form CPGs from the supervirtual data to test for 'flatness'. If the events are horizontal in this domain then the data are likely to satisfy the crucial head-wave assumption. If the raw data have a reasonable SNR, then the corresponding CPGs can be analysed for flatness as well. An example for the field data is given in Fig. 10.

(iii) Compare the supervirtual traveltimes generated from primaries to those generated by multiples; test for agreement (Bharadwaj *et al.* 2011).

(iv) Pick traveltimes from clean records and compare them to those picked from the supervirtual gathers.

The OBS data passed the above tests and details are provided in Bharadwaj *et al.* (2011). Passing these tests is not a guarantee that the supervirtual refractions are not polluted by artefacts, but they significantly reduce the possibility for false results.

5 EXTENSION TO 3D SURVEYS AND EARTHQUAKES

The previous discussion assumed that the source locations, receiver locations and refraction ray paths were in the same plane so that
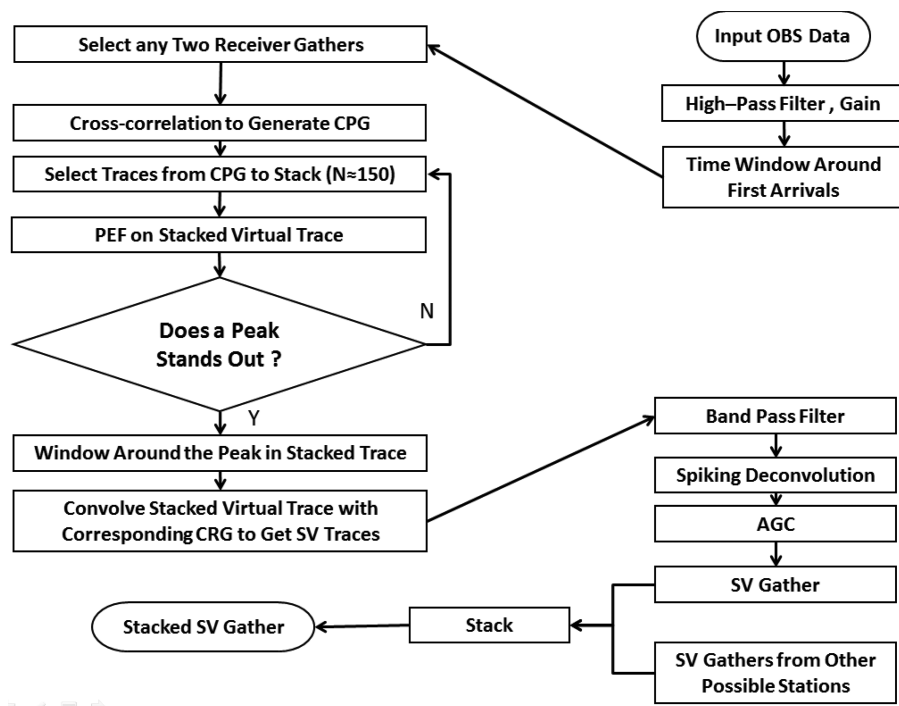
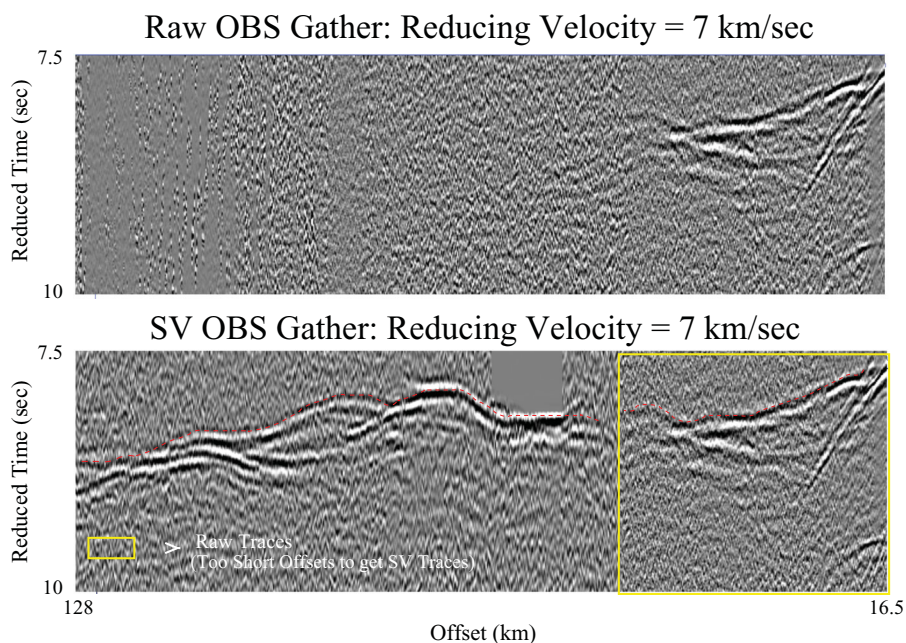**Figure 11.** Flowchart for processing seismic data by SVI.

Figure 12. Top panel: raw, and bottom panel: supervirtual OBS gather from Fig. 9(a) after windowing around the first arrival and applying a time shift to the CRGs with a reduced velocity of 7 km s^{-1}. Arrivals in the yellow box are those of the filtered raw data because the supervirtual traces could not be created at such short offsets.

all post-critical source locations enjoyed the stationary phase property. This stationary phase property for post-critical source locations will not always be true for a 3-D survey where the sources and receivers are not inline with one another. In fact, there are complex velocity models where the post-critical source locations do not enjoy the stationary phase property even if the receivers are inline with the source. In this case, an iterative process might be used to identify the source–receiver locations that enjoy the stationary phase property and enhance the SNR of virtual traces by $\sqrt{N}$. Once

these source–receiver locations are identified then the supervirtual method can be used.

The generation of the virtual traces by correlation of trace pairs removes the source excitation time and the source statics due to an unknown depth of burial. This is ideal for analysing inline records of earthquake records so that the refraction events can be extracted by the supervirtual method. If the earthquake hypocentre is below the Moho, then the refraction event might be generated by a free-surface reflection from the earthquake.

6 CONCLUSIONS

We presented the general theory of supervirtual refraction interferometry where the SNR of far-offset head-wave arrivals can be theoretically increased by a factor proportional to $\sqrt{N}$; here, N is the number of coincident receiver and source positions at post-critical offset. There are two steps to this methodology: correlation and summation of the data to generate traces with virtual head-wave arrivals, followed by the convolution of the data with the virtual traces to create traces with supervirtual head-wave arrivals. This method is valid for any medium that generates head-wave arrivals.

There are at least four significant benefits to this methodology: (1) enhanced SNR of far-offset traces so the first-arrival traveltimes of the noisy far-offset traces can be more reliably picked to extend the useful aperture of data, (2) the SNR of head waves that arrive later than the first arrival can be enhanced for accurate traveltime picking and subsequent inversion by later-arrival traveltime tomography (Mallinson *et al.* 2011) and (3) common receiver-pair gathers (Dong *et al.* 2006) can be analysed to detect the presence of diving waves in the first arrivals, which can be used to assess the nature of the refracting boundary. If supervirtual traces are convolved with virtual traces the SNR enhancement can, in principle, be proportional to N and (4) the source statics term is eliminated in the correlation operations so that the timing of the virtual traces is independent of the source excitation time. This suggests the possibility of applying this method to earthquake data recorded by receivers that are inline with the refraction paths and source locations.

There are at least two potential problems with this method. First, there will be artefacts in the supervirtual traces for a limited recording aperture and a coarse spacing of the source and receivers. This will lead to destructive interference with the supervirtual events. Partial remedies might be dip filtering, windowing about the early arrivals, or least-squares redatuming (Wapenaar *et al.* 2008). Secondly, if the refraction arrivals are primarily diving waves, then, unlike head waves, there are not so many stationary source positions on the surface for a fixed pair of receivers. Hence, the SNR of diving waves will not be greatly increased by this algorithm.

In summary, supervirtual refraction interferometry can be a significant improvement to refraction processing, similar in importance to that of stacking reflections after a normal moveout operation is applied to traces in common midpoint gathers. It can enhance the SNR of head wave arrivals by a factor proportional to $\sqrt{N}$ and can extend the aperture of useful refraction data. If the supervirtual traces, rather than the raw traces, are convolved with the virtual traces then the enhancement of SNR can be as high as N, or more if this is performed in an iterative fashion.

REFERENCES

Bharadwaj, P. & Schuster, G.T., 2010. Extending the aperture and increasing the signal-to-noise ratio of refraction surveys with super-virtual interferometry, *2010 Fall Meeting Am. geophys. Un.*, Abstract S23C-04.

Bharadwaj, P., Schuster, G. & Kirk McIntosh, 2011. Increasing the number and signal-to-noise ratio of OBS traces with super-virtual refraction interferometry and free surface multiples, *Geophys. J. Int.,* submitted.

Braile, L. & Smith, R., 1975. Guide to the interpretation of crustal refraction profiles, *Geophys. J. Int.,* **40,** 145–176, doi:10.1111/j.1365-246X.1975.tb07044.x.

Curtis, A., 2009. Source-receiver seismic interferometry, *SEG Expanded Abstracts,* **28,** 3655–3658, doi:10.1190/1.3255626.

Curtis, A. & Halliday, D., 2010. Source-receiver wave field interferometry, *Phys. Rev. E,* **81**(4), 046601.

Dai, W., Fei, T., Luo, Y. & Schuster, G.T., 2011. Super-virtual interferometric diffractions as guide stars, *SEG Expanded Abstracts,* **30,** 3819–3823, doi:10.1190/1.3628002.

Dong, S., Sheng, J. & Schuster, G.T., 2006. Theory and practice of refraction interferometry, *SEG Expanded Abstracts,* **25,** 3021–3025.

Funck, T., Andersen, M., Neish, J. & Dahl-Jensen, 2008. A refraction seismic transect from the Faroe Islands to the Hatton-Rockall Basin, *J. geophys. Res.,* **113,** B12405, doi:10.1029/2008JB005675.

Halliday, D. & Curtis, A., 2008. Seismic interferometry, surface waves and source distribution, *Geophys. J. Int.,* **175,** 1067–1087.

Mallinson, I., 2010. Investigating the Moho with refraction interferometry, *MSc thesis*, Imperial College, London.

Mallinson, I., Bharadwaj, P., Schuster, G. & Jakubowicz, H., 2011. Enhanced refractor imaging by super-virtual interferometry, *Leading Edge,* **30,** 546–550, doi:10.1190/1.3589113.

Meissner, R., 1973. The Moho as a transition zone, *Surv. Geophys.,* **1,** 195–216, doi:10.1007/BF01449763.

Mooney, W.D. & Weaver, C.S., 1989. Regional crustal structure and tectonics of the Pacific Coastal States: California, Oregon, and Washington, in *Geophysical Framework of the Continental United States*, Geological Society of America Memoir 172, Chapter 9, pp. 129–161, eds Pakiser, L.C. & Mooney, W.D, Geol. Soc. Am., Boulder, CO.

Nichols, J., Mikesell, D.& van Wijk, K., 2010. Application of the virtual refraction to near-surface characterization at the Boise Hydrogeophysical Research Site, *Geophys. Prospect.,* **58,** 1011–1022.

Palmer, D., 1981. An introduction to the generalized reciprocal method of seismic refraction interpretation, *Geophysics,* **46,** 1508–1518, doi:10.1190/1.1441157.

Palmer, D. & Jones, L., 2005. A simple approach to refraction statics with the generalized reciprocal method and the refraction convolution section, *Explor. Geophys.,* **36,** 18–25.

Poliannikov, O., 2011. Retrieving reflections by source-receiver wavefield interferometry, *Geophysics,* **76,** SA1–SA8, doi:10.1190/1.3524241.

Schuster, G.T., 2009. *Seismic Interferometry,* Cambridge University Press, Cambridge.

Sheriff, R. & Geldart, L., 1995. *Exploration Seismology,* Cambridge University Press, Cambridge.

Slob, E., Draganov, D. & Wapenaar, K., 2007. Interferometric electromagnetic Green's functions representations using propagation invariants, *Geophys. J. Int.,* **169,** 60–80.

Snieder, R., 2004. Extracting the Green's function from the correlation of coda waves: A derivation based on stationary phase, *Phys. Rev. E,* **69,** 046610.

Wapenaar, K., 2004. Retrieving the elastodynamic Green's function of an arbitrary inhomogeneous medium by cross correlations, *Phys. Rev. Lett.,* **93,** 254301.

Wapenaar, K., 2007. General representations for wavefield modeling and inversion in geophysics, *Geophysics,* **72,** SM5–SM17.

Wapenaar, K. & Fokkema, J., 2006. Green's function representations for seismic interferometry, *Geophysics,* **71,** SI33–SI46.

Wapenaar, K., van der Neut, J. & Ruigrok, E., 2008. Passive seismic interferometry by multidimensional deconvolution, *Geophysics,* **73,** A51, doi:10.1190/1.2976118.

Xue Y. & Schuster, G.T., 2008. Least squares datuming with the wave equation, *SEG Expanded Abstracts,* **25,** 2366–2370.

Xue, Y., Dong, S. & Schuster, G.T., 2009. Interferometric prediction and subtraction of surface waves with a nonlinear local filter, *Geophysics,* **74,** SI1–SI8.

Yilmaz, O., 2001. *Seismic Data Analysis,* 2nd edn, SEG Publishing, Tulsa, OK.

Zelt, C. & Smith, R., 1992. Seismic travel time inversion for 2-D crustal velocity structure, *Geophys. J. Int.,* **108,** 16–34.

Zhu, X., Sixta, D. & Angstam, B., 1992. Tomostatics: turning-ray tomography + static corrections, *Leading Edge,* **11**(12), 15–23.